
Proceedings Paper:
Sun, C., Kengne, P.L.F., Barrios, A. et al. (2 more authors) (2019) Form error prediction in robotic assisted milling. In: Ozturk, E., Mcleay, T. and Msaoubi, R., (eds.) Procedia CIRP. 17th CIRP Conference on Modelling of Machining Operations (17th CIRP CMMO), 13-14 Jun 2019, Sheffield, UK. Elsevier , pp. 491-496.

https://doi.org/10.1016/j.procir.2019.04.335

Available online at www.sciencedirect.com

ScienceDirect

Procedia CIRP 82 (2019) 491–496

www.elsevier.com/locate/procedia

17th CIRP Conference on Modelling of Machining Operations

Form Error Prediction in Robotic Assisted Milling

Chao Sun[a], Patrick L. F. Kengne[a], Asier Barrios[b], Sara Mata[b], Erdem Ozturk[a]*

[a] AMRC with Boeing, the University of Sheffield, Sheffield S60 5TZ, UK
[b] IK4 Ideko, Elgoibar, Spain

* Corresponding author. Tel.: +44 (0)114 222 6671 . *E-mail address:* e.ozturk@sheffield.ac.uk

Abstract

Robotic assisted milling is a process where a robot supports a workpiece while a machine tool cuts the workpiece. It can be used to suppress vibrations and minimize form errors in thin wall workpieces. In this paper, form error on a workpiece is simulated using a static force model, a frequency domain model and a hybrid model while a robot supports the workpiece from the other side. Machining results show that assistance of the robot has a considerable effect of the magnitude of form errors. Hence, support force should be carefully selected by simulation before machining. Finally, simulation results show that hybrid model gives the best fit among those three models.

Peer-review under responsibility of the scientific committee of The 17th CIRP Conference on Modelling of Machining Operations

Keywords: robotic assisted milling; form error; thin-wall machining.

1. Introduction

Light weight structures, also known as thin walled parts, are very commonly used in the aerospace sector. The machining times of these components are usually limited by chatter vibrations that occur due to low stiffness of the parts. Milling stability theory [1] can be used to eliminate chatter and increase productivity by optimizing machining parameters such as spindle speed and depth of cut. To further improve the productivity, dynamic response of the thin-wall structure needs to be improved.

To improve the dynamic response of the workpiece, fixturing of the part has been investigated. Two kinds of support methods, fixed support [2–4] and mobile support [5–7], are proposed. Compared to fixed support, the advantage of mobile support is that the support on the part will be very close to the cutting zone throughout the process as the support is following the motion of the milling tool. Mtorres machine tool company designed a special surface milling machine [5]. This machine has special apparatus support the component on the opposite side of machining. Fei et al. [6] developed an mobile support attached to the spindle housing of a machine tool. It showed that mobile support increased the stability of the process. Ozturk et al. proposed robotic assisted milling [7], where a robot provides mobile support while a machine tool performs milling operation, provides an flexible and reconfigurable solution.

The support force provided by mobile fixture will cause deflection of the part, which will influence the form error of the machined surface. To find proper magnitude of the support force, a form error model for machining process with mobile fixture need to be developed. For traditional machining process which do not have extra support force, the form error prediction model has been investigated in both time domain[8,9] and frequency domain[10]. However, a form error model has not been developed yet for a machining process with mobile fixture.

In this paper, three different form error prediction models for robotic assisted machining are proposed and compared. In Section 2, these three models are introduced in detail. In Section 3, machining tests results are compared with simulation results.

2212-8271
Peer-review under responsibility of the scientific committee of The 17th CIRP Conference on Modelling of Machining Operations
10.1016/j.procir.2019.04.335

2. Form error modelling

In this section, different models to predict form errors are introduced. It begins with the model using static stiffness. Then the model using dynamic response is discussed. Finally, model combining both static stiffness and dynamic stiffness is proposed. It should be noted here that these models are for thin-wall parts and only the deflection of workpiece is considered.

2.1. Static deflection model

In this part, a form error model using static stiffness is presented. First, the cutting force calculation method is introduced. Then the equations to calculate the form error are presented.

The cutting tool can be discretized into M number of small disks along tool axis within the axial depth of cut a. As shown in Fig. 1, the form error in milling process is only influence by the cutting force in Y direction. The cutting force $F_{y,m}(\phi)$ for each disk in Y direction can be calculated by Equation (1), where K_{tc} is tangential cutting force coefficient, K_{rc} is radial cutting force coefficient, K_{te} is tangential edge force coefficient, K_{re} is radial edge force coefficient, f_t is the feedrate, $j = 1,2,\dots N$ is the flute index and ϕ is the instantaneous angle of immersion.

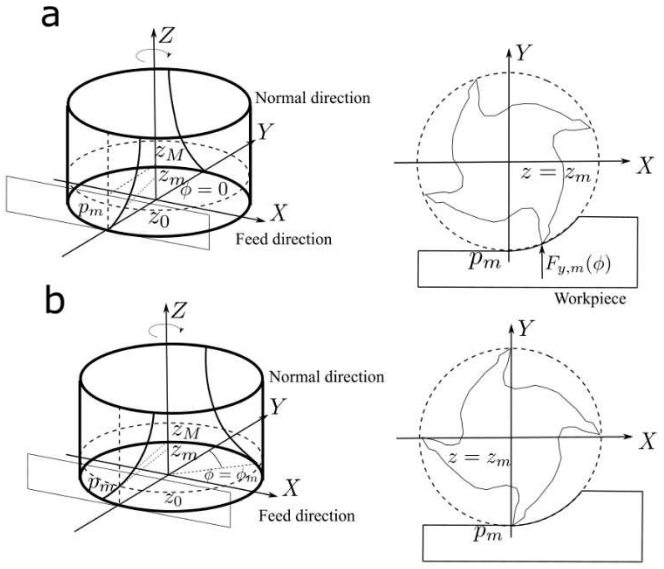

Fig. 1. Geometry of helical end mill. (a) $\phi = 0$; (b) $\phi = \phi_m$.

$$F_{y,m}(\phi) = \frac{a}{M}\sum_{j=1}^{N}\{f_t[K_{tc}\sin\phi_j - K_{rc}\cos\phi_j]\sin\phi_j + [K_{te}\sin\phi_j - K_{re}\cos\phi_j]\} \quad (1)$$

The total instantaneous cutting force in Y direction that sums the contribution of each disc can be calculated by Equation (2).

$$F_y(\phi) = \sum_{m=1}^{M} F_{y,m}(\phi) \quad (2)$$

As shown in Fig. 1, the flute pass the surface of workpiece at different instantaneous angle of immersion ϕ. ϕ_m for each disk can be calculated by Equation (3), in which β is the helix angle, R is the radius of cutter, z_m is the height of point p_m.

$$\phi_m = \frac{z_m \tan\beta}{R} \quad (3)$$

For each flute j, the instantaneous angle $\phi_{m,j}$ can be calculated by Equation (4), in which ϕ_p is the cutter pitch angle.

$$\phi_{m,j} = \phi_m + (j-1)\phi_p \quad (4)$$

Then the instantaneous cutting force in Y direction at which the flute pass point p_m can be calculated by Equation (2).

As shown in Fig. 2, in robotic assisted machining, the forces cause the deflection of the workpiece are composed of the cutting forces from the machining process and the support force from robot. Therefore,δ_m, the form error at point p_m, can be calculated by Equation (5). F_C is the cutting force on workpiece in surface normal direction, which is Y direction of cutting tool in Fig. 1. F_S is the support force and k is the static stiffness of workpiece. It should be noted that the positive result of δ_m means under cut, while the negative result of δ_m means over cut.

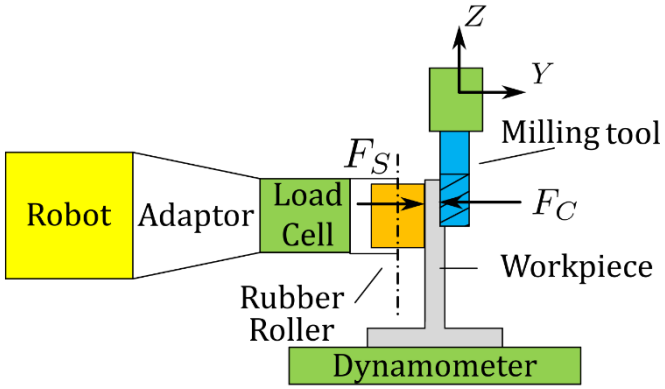

Fig. 2. Setup of robotic assisted machining.

$$\delta_m(t) = \frac{F_C - F_S}{k} = \frac{F_y[\phi(t_m)] - F_S}{k} \quad (5)$$

2.2. Frequency domain model

In this part, the frequency domain model is presented.

The force applied on workpiece in Y direction can be expressed in Equation (6), in which F_C is the cutting force and F_S is the support force (Fig. 2).

$$F_w(\phi) = F_C - F_S = -F_y(\phi) - F_S \quad (6)$$

It can be expressed in frequency domain using a Fourier series as presented in Equation (7).

$$F_w(\omega) = \mathcal{F}[F_w(t)] = \mathcal{F}\{F_w[\phi(t)]\} \quad (7)$$

Then the vibration of workpiece in frequency domain can be calculated using Equation (8), where Φ(ω) is the frequency response function of workpiece.

$$\delta(\omega) = F_w(\omega)\Phi(\omega) \quad (8)$$

The vibration of workpiece in time domain $\delta(t)$ can be calculated through inverse Fourier transform of $\delta(\omega)$.
Finally, the form error at point p_m can be calculated by Equation (9), where t_m is the time when the flute pass the point p_m and ω_n is spindle speed in rad/s.

$$\delta_m = \delta(t_m) = \delta(\phi_m/\omega_n) \quad (9)$$

2.3. Hybrid model

In this part, a method using both static stiffness and dynamic frequency response is presented.

During robotic assisted machining process, the deflection is caused by both cutting forces and support force. The support force applies a static force, while the cutting forces apply dynamic forces. Therefore, the deflection from support force can be calculated using Equation (10).

$$\delta_{m,S} = \frac{F_S}{k} \quad (10)$$

The deflection caused by cutting force $\delta_{m,C}$ can still be calculated using Equation (7)~(9) by substituting the total force on workpiece $F_w[\phi(t)]$ with the cutting force $F_y[\phi(t)]$.

The total form error can be calculated as follows:

$$\delta_m = \delta_{m,S} + \delta_{m,C} \quad (11)$$

The differences among three models are shown in Fig. 3. In static model, the form error is calculated based on static stiffness. The influence of dynamic behavior of the workpiece is ignored. In frequency domain model, the force (F_w) applied on workpiece is firstly calculated by adding the support (F_S) to cutting forces (F_C). Then the form error is calculated with F_w and workpiece FRF from tap test. In hybrid model, the form errors caused by support force and cutting forces are calculated separately. Static stiffness from direct measurement, which is expected to be more accurate than static stiffness estimated from FRF from tap test, is utilized to calculate the form error from support force. The total form error is calculated from the sum of form errors from support force and cutting forces. It should be noted that FRF change due to material removal in cutting is not considered in this paper.

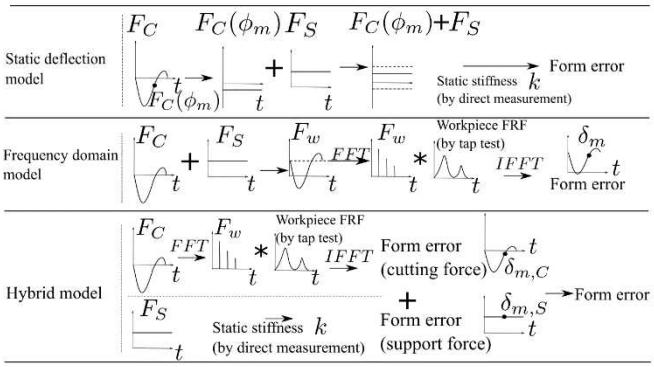

Fig. 3. Comparison of three models.

3. Experiment and simulation result

3.1. Test set-up

In the test set-up, a Staubli TX90 robot was installed to provide support force for machining process on a Starrag STC1250 5-axis milling machine. A rubber roller was assembled on to the end effector of the robot. A Kistler 9317C load cell was positioned between the adapters to be able to measure the support force F_S. The support force F_S is sent back to robot to control the support force. The milling tool (Sandvik R216.32-20025-AP20A H10F) was a 20 mm diameter carbide end mill with 2 flutes. The workpieces were T-profiles from Aluminium 6082-T6, of which height, thickness and length were 101.6, 9.5mm and 250mm, respectively. The workpieces were clamped to the Kistler 9255C dynamometer to measure forces on the workpiece (Fig. 4). Workpiece frame (X_W, Y_W, Z_W) and process frame (X, Y, Z) are shown in Fig. 4.

Cutting tests were performed with different support forces to demonstrate its effect on form errors. For each trial, a new T-profile workpiece was used. In these tests, down milling were used. Spindle speed and feed per tooth was 7000rpm and 0.1mm/tooth, respectively. 2mm radial depth of cut and 10mm axial depths of cut were used.

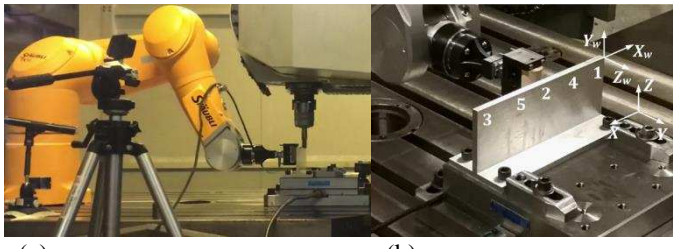

(a) (b)

Fig. 4. (a) Experimental set-up (b) measurement points.

3.2. FRF, stiffness and cutting force

Direct transfer functions were measured in five different locations by tap test for no support, 120N support and 200N support. Fig. 5 shows the result of G11, G22 and G44 with 120N support force. It shows that the transfer functions varies along the X_W axis. The transfer functions at point 1 with no support, 120N support and 200N support are shown in Fig. 6.

Higher dynamic stiffness was seen for cases with support. The change of support force doesn't show significant influence on FRF. Compared to the difference between the FRF result with support and that without support, the difference between the FRF results with 120N support and that with 200N support is relatively small.

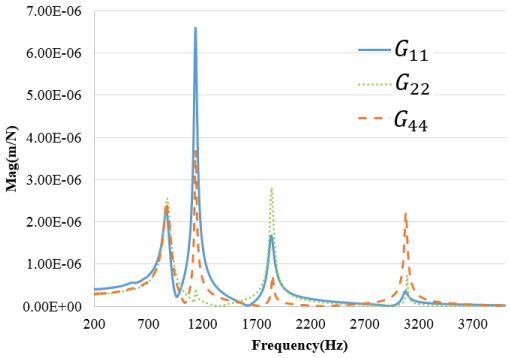

Fig. 5. Direct frequency response function G_{11}, G_{22}, G_{44} with 120N support force.

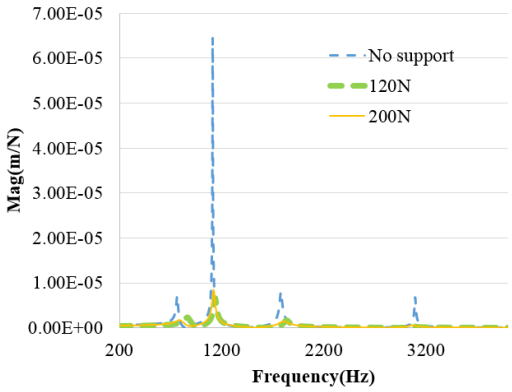

Fig. 6. Direct frequency response function G_{11}.

The static stiffness of workpiece were measured using laser displacement sensor and load cell (Table 1).

Table 1. Static stiffness results.

No.	Position in X_W (mm)	Stiffness (N/mm)
P1	-10	2500
P4	-67.5	3333
P2	-125	5000
P5	-182.5	3333
P3	-240	2500

The cutting force is first simulated for the simulation of form error. Acquired from cutting force coefficient test, the cutting force coefficient *Ktc* and *Krc* are 1168N/mm^2 and 632N/mm^2 respectively. The edge force coefficient *Kte* and *Kre* are 0.75N/mm and 0.27N/mm respectively. Fig. 7 shows the simulation and the measurement of cutting forces in *Zw* (*Y* direction of tool). The maximum cutting force from measurement is 467N and that from simulation is 430N. From the simulation, When the flute of the tool pass the points at Y_W=-6mm, the force in *Zw* (*Y* direction of tool) is 70N.

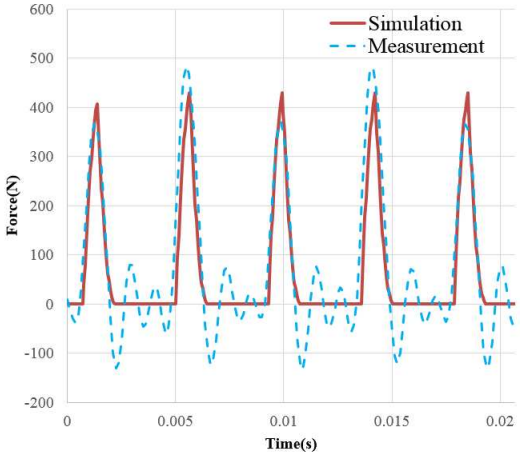

Fig. 7. Cutting force result for test with no support.

3.3. Form error

The form errors were measured using an on machine probe with 20 mm increments along the length of the workpiece between -10mm and -230mm along the workpiece coordinate *Xw* (Fig. 4). The probing points were 6 mm below the top face of the workpiece (*Yw*=-6mm). As shown in Fig. 8, support forces showed large influences on the form errors. Although the same support force is applied, the form error varies among different points because the FRF varies along the workpiece (Fig. 5).

In this case, the smallest form error is with 280N support. It should be noted that it is not necessarily that larger support force will lead to lower form error, as the form error with no support could be negative in some cases, for example, sometimes in up milling case.

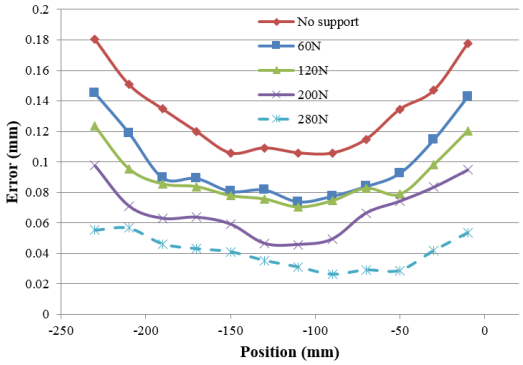

Fig. 8. Form errors results from measurement.

Simulation results using static model for no support, 120N support and 280N support are shown in Fig. 9. The results for no support test presented in Fig. 9 show that the static model underestimate the form error caused by cutting force. The maximum difference is 0.149mm. For 120N support and 280N,

the curve shape of the simulation results are different from the measurement results.

Using the dynamic model, simulations are done from point 1 to point 5. Simulation results using dynamic model for no support, 120N support and 280N support are shown in Fig. 10. Fig. 10 shows that the maximum error for no support test is 0.038mm, which is a positive value. However, for 280N support force, the maximum error is -0.069mm. It can be seen that the errors of the simulation change from positive to negative with the increase of support force. The reason could be, in dynamic model, the static stiffness is estimated from FRF from tap test result, which may not be as accurate as direct measurement of static deflection. In contrast, static stiffness values listed in Table 1 are used in hybrid model.

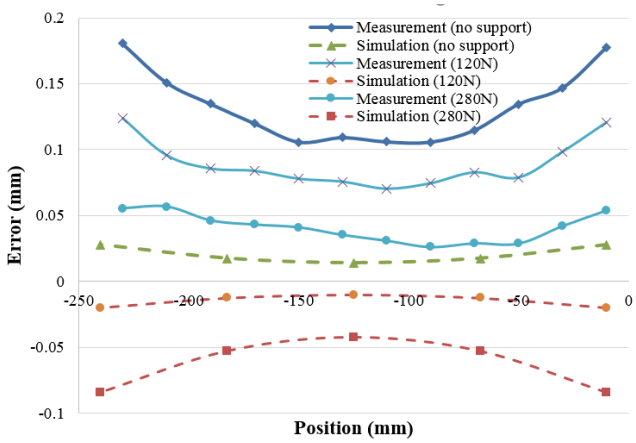

Fig. 9. Simulation using static deflection model and measurement results.

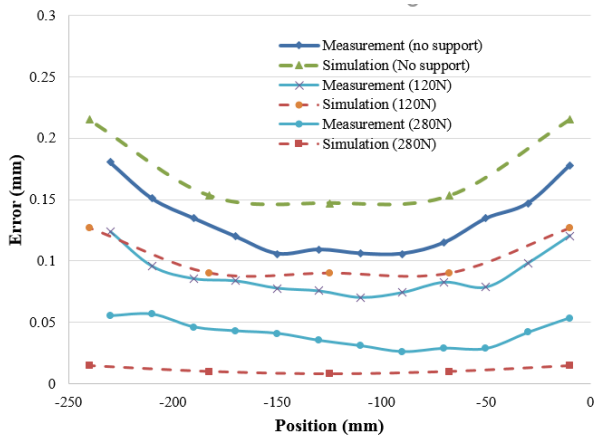

Fig. 10. Simulation using frequency domain model and measurement results.

For no support simulation, hybrid model and frequency domain model is the same. The simulation results for 120N support and 280N support are shown in Fig. 11. The simulation results show relatively consistent positive errors.

Table 2 compares the maximum error of each model. The static model shows the largest maximum error for all of the cases. The dynamic deflection model shows smallest maximum error for 120N case. However, the sign of the error changes when the support force increases in dynamics model.

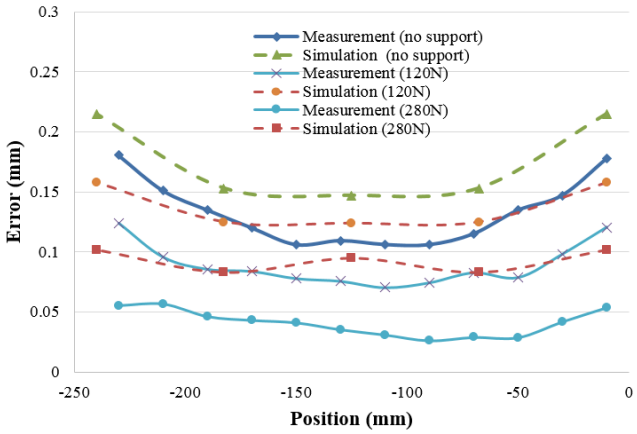

Fig. 11. Simulation using hybrid model and measurement results.

Table 2. Maximum simulation errors of each model.

	No support	120N support	280N support
Static deflection model	-0.149mm	-0.103mm	-0.137mm
Dynamic deflection model	0.038mm	0.015mm	-0.069mm
Hybrid model	0.038mm	0.049mm	0.06mm

The maximum error from hybrid model keeps positive, which is more reasonable. These consistent positive errors could come from cutter radius error, machine tool positioning error and measurement errors. In this test, the machine tool positioning accuracy is 0.005mm. The maximum radius error of the tool, including the runout, is 0.014mm. These two may introduce form errors. The probing tool itself has a high accuracy, which is around 0.001mm. However, as the probing is done on machine tool, the machine tool positioning accuracy will also bring in the measurement errors.

4. Conclusion

Three methods for calculating form errors for robotic assisted milling are developed in the paper. A few conclusions can be acquired from the results in this paper. Firstly, the support force in robotic assisted machining can change the form error. Therefore, form error should be simulated and support force should be carefully selected. Second, among all three methods, hybrid model shows more reasonable results. Compared to static model and frequency domain model, hybrid model gives relatively consistent differences with the measurement. Finally, measurement results show that the form errors are different at different points with constant support force on the workpiece. For example, the form errors on point 1 and point 2 show different values. This is because the dynamic and static stiffness are different at each point. Therefore, to achieve a constant form error on a workpiece, a profile of support forces should be calculated and applied at different positions on workpiece.

Acknowledgements

The authors would like to acknowledge the funding provided by the European Commission under the Horizon 2020 Programme to the COROMA project under grant agreement no. 723853. Companion information to the paper is available at the project's Zenodo repository under https://zenodo.org/communities/coroma-project.

References

[1] Y. Altintas, Manufacturing Automation, in: Cambridge University Press, 2012. doi:10.1017/CBO9780511843723.001.
[2] X.-J. Wan, Y. Zhang, A novel approach to fixture layout optimization on maximizing dynamic machinability, Int. J. Mach. Tools Manuf. 70 (2013) 32–44. doi:10.1016/j.ijmachtools.2013.03.007.
[3] K. Kolluru, D. Axinte, A. Becker, A solution for minimising vibrations in milling of thin walled casings by applying dampers to workpiece surface, CIRP Ann. 62 (2013) 415–418. doi:10.1016/j.cirp.2013.03.136.
[4] A. Matsubara, Y. Taniyama, J. Wang, D. Kono, Design of a support system with a pivot mechanism for suppressing vibrations in thin-wall milling, CIRP Ann. 66 (2017) 381–384. doi:10.1016/j.cirp.2017.04.055.
[5] Mtorres, Torres Surface Milling, (n.d.). https://goo.gl/Sd7bNP (accessed December 20, 2019).
[6] J. Fei, B. Lin, S. Yan, M. Ding, J. Xiao, J. Zhang, X. Zhang, C. Ji, T. Sui, Chatter mitigation using moving damper, J. Sound Vib. 410 (2017) 49–63. doi:10.1016/j.jsv.2017.08.033.
[7] E. Ozturk, A. Barrios, C. Sun, S. Rajabi, J. Munoa, Robotic assisted milling for increased productivity, CIRP Ann. 67 (2018) 427–430. doi:10.1016/j.cirp.2018.04.031.
[8] D. Montgomery, Y. Altintas, Mechanism of Cutting Force and Surface Generation in Dynamic Milling, J. Eng. Ind. 113 (1991) 160. doi:10.1115/1.2899673.
[9] T. Schmitz, J. Ziegert, Examination of surface location error due to phasing of cutter vibrations, Precis. Eng. 23 (1999) 51–62. doi:10.1016/S0141-6359(98)00025-7.
[10] T.L. Schmitz, B.P. Mann, Closed-form solutions for surface location error in milling, Int. J. Mach. Tools Manuf. 46 (2006) 1369–1377. doi:10.1016/j.ijmachtools.2005.10.007.